Applied Physics A (2022) 128:692
https://doi.org/10.1007/s00339-022-05821-5

Applied Physics A
Materials Science & Processing

Check for updates

Low-cost hydrogen peroxide sensor based on the dual fluorescence of *Plinia cauliflora* silver nanoparticles

Karina de Oliveira Gonçalves[1] · Flavia Rodrigues de O. Silva[2] · Lilia Coronato Courrol[1]

Received: 12 November 2021 / Accepted: 24 June 2022 / Published online: 18 July 2022

Abstract

A low-cost and reliable detection of hydrogen peroxide is essential in the pharmaceutical, medical, and food industries, since H_2O_2 can cause irreversible cellular damage through the oxidation of biomolecules. This paper describes a sensitive luminescent sensor for H_2O_2 based on a dual fluorescence-colorimetric assay for determining the hydrogen peroxide using silver nanoparticles prepared with *Plinia cauliflora* extracts (*Pc*AgNPs). Nanoparticles were characterized by UV–Vis, transmission electron microscopy, elemental analysis, Zeta potential, FTIR, and fluorescence. The average size of spherical particles was ~ 14 nm. The photoreduction process and pH control improved the nanoparticle's photophysical properties and stability. With pH adjustment, the Zeta potential of *Pc*AgNPs prepared with fruit extract changed from ~ − 17 mV to ~ − 30 mV. The behavior of the *Pc*AgNPs SPR and fluorescence bands were studied in the presence of H_2O_2. The SPR band of *Pc*AgNPs around 420 nm gradually decreased upon the increasing concentration of H_2O_2, while the *Pc*AgNPs emission has an enhancement and a shift (from ~ 470 to ~ 440 nm) in the presence of hydrogen peroxide. A calibration curve was obtained in the range of 0–5 μM, with a calculated detection limit of 0.15 μM. The present biosensor can be applied as an alternative method for detecting hydrogen peroxide in medical care and environmental monitoring.

Keywords *Plinia cauliflora* · Silver nanoparticles · FTIR · UV–Vis · Photoreduction · Fluorescence · Hydrogen peroxide

1 Introduction

Hydrogen peroxide (H_2O_2) is a reactive oxygen species (ROS) and plays a vital role in many biological processes and enzymatic reactions[1]. This compound is employed in several industrial sectors for bleaching and sterilizing procedures in the food industry, water treatment, and biochemical practices[2–4]. Nowadays, H_2O_2 has been employed as a disinfection adjuvant to mitigate the risk of indirect SARS-CoV-2 spreading [5]. H_2O_2 can cause intracellular oxidative stress associated with aging, neurodegeneration, and cancer[6, 7]. For this reason, an accurate and low-cost method to detect H_2O_2 in vitro and in vivo has become necessary[8].

✉ Lilia Coronato Courrol
lcourrol@unifesp.br

[1] Instituto de Ciências Ambientais, Químicas e Farmacêuticas, Departamento de Física, Universidade Federal de São Paulo, Diadema, São Paulo, Brazil

[2] Centro de Ciências e Tecnologia dos Materiais, Instituto de Pesquisas Energéticas e Nucleares, IPEN/CNEN-SP, São Paulo, SP, Brasil

Various analytical methods have been applied to determine hydrogen peroxide, including fluorescence and colorimetric assays[9–11]. Fluorescence sensors exhibit changes in emission intensity or shifts in the emission profiles[12, 13]. However, naked-eye detection or colorimetric detection is most preferred because of its simplicity, low costs, and fast response[14].

Silver nanoparticles (AgNPs) have been used for sensing applications [15–18]. Colorimetric detection of H_2O_2 using AgNPs has been described[17, 19]. However, the use of fluorescence spectroscopy of plant-synthesized AgNPs to detect variations in H_2O_2 content in a solution was not reported.

AgNPs possess strong surface plasmon resonance (SPR) absorption of around 420 nm depending on their size, shape, composition, and the surrounding media[20]. The environmentally friendly and sustainable synthesis methods like green synthesis using plant extracts[21, 22] or microorganisms [23] and physical methods such as pulsed laser ablation[18, 24, 25] and photoreduction [26–28] have been employed to synthesize AgNPs of variable sizes and shapes.

Compared to chemical methods, photochemical routes in nanotechnology are advantageous, because they avoid the use of toxic or harmful compounds, allow spatial and temporal control, do not depend on expensive instrumentation or highly qualified personnel, and, most importantly, can be performed under environmental conditions [28–31]. The photochemical process begins with the reduction of the metallic precursor, from (Ag+) to its zero valence state (Ag^0) by the photocatalyzed action of the reducing agent. The Ag^0 form nucleation centers or nuclei that later grow and aggregate to give rise to AgNPs.

In 2003, plant-based synthesis of silver nanoparticles was published using *Medicago sativa* [32]. After this publication, several other studies were performed using plant extracts to obtain silver nanoparticles [33–36]. Synthesis of nanoscale materials using plant extracts attracts attention as it is a simple, effective, cheap, and feasible method for obtaining nanoparticles. Biologically active compounds found in plants can reduce metal ions much faster than bacteria or fungi. Polyphenols compounds, such as flavonoids and phenolic acids, are among the essential phytochemicals responsible for the nanoparticle's bioreduction [37]. These compounds can reduce silver ions and, at the same time, act as a capping agent stabilizing the nanoparticles [38]. The photoreduction method can improve the optical quality of AgNPs prepared with plant extracts[28, 39].

Recently, several publications on *Plinia cauliflora* have attracted considerable attention since the fruits and leaves of this plant present antioxidant, anti-inflammatory, antimicrobial, and anti-cancer activities [40–44]. *P. cauliflora* (Mart.) Kausel is a tree in the family *Myrtaceae* that includes about 5900 species. These species are found in Brazil's Atlantic rainforest, Pantanal, Cerrado, and Caatinga biomes [45]. The tree is 10–15 m tall with single leaves up to 7 cm long and blooms in the spring and summer (Fig. 1a). The flowers and fruits (jabuticaba) grow in clusters along the trunk and branches. Jabuticaba is sweet, pleasant to taste, and rich in phenolic constituents, anthocyanins, flavanols, and ellagitannins [44]. Traditionally jabuticaba is used for the treatment of diarrhea, asthma, chronic inflammation of the tonsils, etc. [41, 42, 46]. There is no report on the synthesis of AgNPs mediated by *P. cauliflora* extracts.

In this paper, the *P.cauliflora* extracts, photoreduction method, and pH control were employed to obtain AgNPs with excellent optical properties. The nanoparticles were characterized by UV–Vis, transmission electron microscopy, elemental analysis, FTIR, and fluorescence spectroscopy. Furthermore, the H_2O_2 detection was described based on the reduction of the SPR band (colorimetric method) or/and the increase in the fluorescence intensity of *Pc*AgNPs. Method sensitivity was obtained.

2 Materials and methods

2.1 Materials and synthesis

Silver nitrate ($AgNO_3$) was purchased from Sigma-Aldrich. *P. cauliflora* leaves and fruits were collected from a spontaneous germination tree in São Paulo, SP, Brazil. All solutions were prepared with double-distilled water under ambient conditions.

P. cauliflora leaves and fruits were repeatedly washed with double-distilled water. Leaves or fruits (1.040 ± 0.025 g) were finely chopped and boiled for 5 min in 100 mL of double-distilled water. After 1 min, the solutions were filtered, and two mmol of $AgNO_3$ was added to the extracts at ~ 80 °C to prepare silver nanoparticle solutions (*Pc*AgNPs). After the reaction, the suspensions became acidic (pH $\cong 3.9 \pm 0.3$). The pH of prepared solutions was adjusted to neutral with sodium hydroxide (NaOH). Solutions containing $AgNO_3$ and *P. cauliflora* extracts were submitted to the photoreduction process to improve nanoparticle properties (Table 1). In this case, 10 mL of solutions were exposed to a 300 Watt xenon

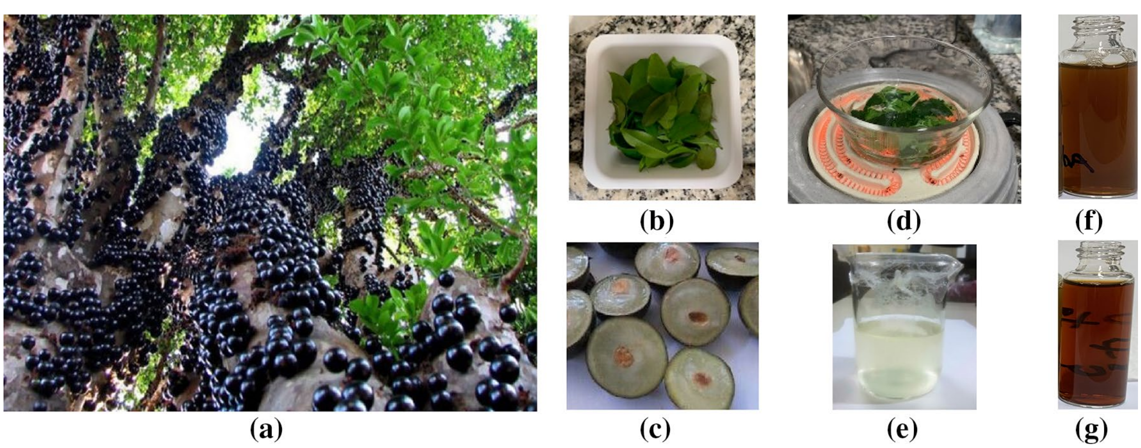

Fig. 1 **a** Jabuticaba tree, **b** *P. cauliflora* leaves, **c** jabuticaba, **d** leaves infusion, **e** extract from *P. cauliflora* leaves, **f** *Pc*AgNP 2, **g** *Pc*AgNP 6

Table 1 Prepared samples. Reagents concentrations and method

Sample	Leaves	Fruits	$AgNO_3$	Light (min)	pH
Pc leaves extract	1.1 g				
Pc fruits extract		1.1 g			
PcAgNP1	1.1 g		2 mmol		
PcAgNP 2	1.1 g		2 mmol		7.0
PcAgNP 3	1.1 g		2 mmol	1 min Xe	
PcAgNP 4	1.1 g		2 mmol	1 min Xe	7.0
PcAgNP 5		1.1 g	2 mmol		
PcAgNP 6		1.1 g	2 mmol		7.0
PcAgNP 7		1.1 g	2 mmol	1 min Xe	
PcAgNp8		1.1 g	2 mmol	1 min Xe	7.0

lamp (Cermax) for 1 min. After the photoreduction process, pH was adjusted to neutral. Some pictures of the synthesis process are shown in Fig. 1.

2.2 Characterization of nanoparticles

Spectrophotometry in the UV–Vis region was performed with the Shimatzu MultiSpec 1501 spectrophotometer. In this case, 50 µL of *Pc*NPs were diluted in 500 µL of doubly distilled water, and the measurements were carried out in a 10 mm optical path quartz cuvette in the range of 200 and 800 nm.

The colloidal suspension's zeta potential and size were analyzed using the Zetasizer Nano ZS Malvern. Three assays were made for each sample.

The Fourier transform infrared spectroscopy (FTIR) was obtained with Shimatzu IRPrestige. In this case, 200 µL of the *Pc*NPs and their extracts were deposited on microscope slides and dried in an oven at 60°. The process was repeated three times. The material deposited on the blades was scraped off to make KBr pellets.

The JEM 2100 JEOL microscope obtained transmission electron microscopy images and elemental analysis.

Fluorescence measurement was recorded on an RF-5301PC Shimatzu fluorimeter. The fluorescence spectra were accomplished on a 1 × 1 cm quartz cell at excitation at 320 nm.

2.3 Determination of hydrogen peroxide calibration curve

Hydrogen peroxide solutions were prepared in deionized water. 1 mL of hydrogen peroxide solution (0–5 pM) was added to 1 mL of *Pc*AgNP6. The reaction was done at room temperature and finished after 30 min. With the increasing H_2O_2 concentration, the *Pc*AgNPs solution color changed from yellow to transparent. A standard calibration curve was obtained from *Pc*AgNp6 intensity fluorescence (at 470 nm) behavior exciting samples at 320 nm.

2.4 Selectivity for H_2O_2

To determine the selectivity of the method, fluorescence analysis were performed with *Pc*AgNP6 in the presence of Ba^{2+}, Ca^{2+}, Cd^{2+}, Co^{2+}, Cu^{2+}, K^{+}, Li^{+}, Mg^{2+}, Na^{+}, Sr^{2+}, Zn^{2+} cations (from Vetec) at a concentration of 100 µg/mL (± 3 µg/mL) incubated for 30 min. Interference of glucose (Glucose PAP SL, from ElitechGroup), cholesterol (Cholesterol solution, from ElitechGroup), triglycerides (Triglycerides Mono SL, from ElitechGroup), urea peroxide (Urea hydrogen peroxide from Aldrich), tryptophan (Tryptophan P.A. from Vetec), and human saliva (56 years old healthy woman) were also determined. 100 µL of solutions were mixed with 2 mL of *Pc*AgNP6 (100 µM).

3 Results

3.1 PcNPs' synthesis and characterization

Extracts of *P. cauliflora* leaves and fruits present absorption bands in the UV region attributed to polyphenols like flavonoids, tannins, etc., as observed in Fig. 2a [47]. Leaf extract presents absorption bands at 233 nm (A-ring absorption) and $\lambda = 349$ nm (B-ring absorption) that can be assigned to flavonoids like quercetin and a band at 277 nm of tannic acid[48]. The absorption bands of fruit extract are considerably more intense than leaf extract. The fruit extract bands centered at 247 nm and 375 nm, with a shoulder around 305 nm, are attributable to ellagic acid (EA)[49]. The exhibited absorption peak around 420 nm in the visible region may be due to chlorophyll absorption. The anthocyanins absorb light between 460 and 550 nm and are responsible for fruit color.

The UV–Vis spectra of the *Pc*AgNPs prepared with leaf and fruit extracts are shown in Fig. 2b, c. In both cases, SPR bands around 430 nm can be observed, indicating the formation of the *Pc*AgNPs immediately after adding $AgNO_3$ to the extracts. After exposure to Xenon light for only 1 min, the SPR band intensity increases. With the pH adjustment to 7.0, a blue shift (to ~ 420 nm) of the *Pc*AgNPs SPR band is observed. The full width at half maximum (FWHM) of the SPR band describes the polydispersity of the solution. A narrow SPR band is observed in Fig. 2c for nanoparticles prepared with fruit extract by photoreduction (~ 399 nm), indicating that these nanoparticles are more homogeneous and smaller. The optical density is almost three times higher for the samples prepared with fruit extract than those prepared with leaf extract (Fig. 2c). This effect indicates that fruit extract prepared AgNPs are more concentrated than leave extract

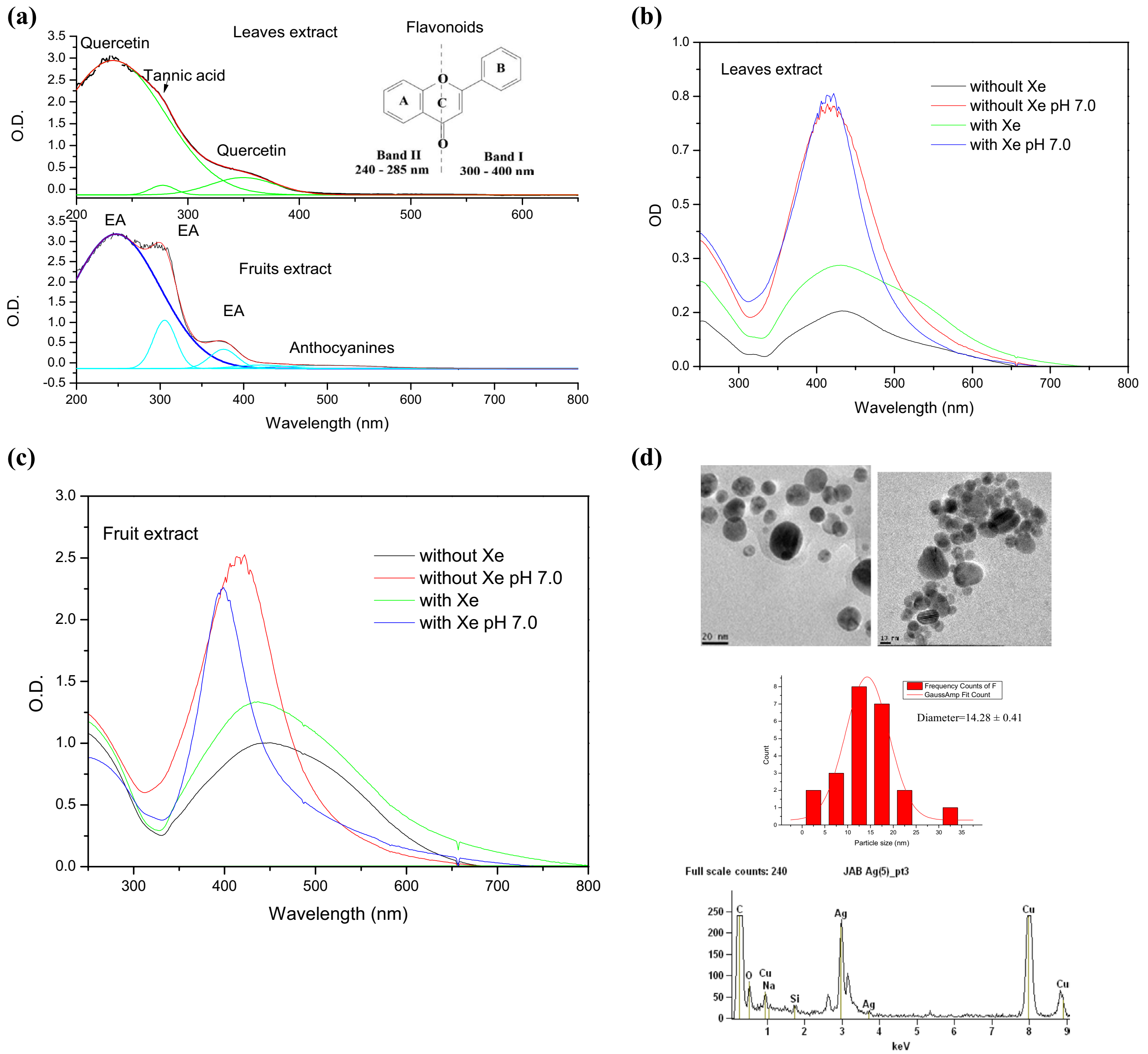

Fig. 2 **a** UV–Vis spectra of leaf and fruit extracts. **b** UV–Vis spectra of *Pc*AgNPs (leaf extract) before and after irradiation with Xenon lamp by 1 min and pH adjustment. **c** UV–Vis spectra of *Pc*AgNPs (fruit extract) before and after irradiation with Xenon lamp by 1 min and pH adjustment. **d** TEM images of *Pc*AgNP6, size distribution, and elemental analysis of synthesized particles to show the Ag or other elements present in the sample. Accelerating voltage: 200.0 kV Magnification: 100,000

prepared AgNPs. Figure 2d shows the TEM images of *Pc*AgNP6, indicating particles with diameters of ~ 14 nm, and the elemental analysis indicated the presence of Ag in the samples.

Zeta potential measurements were performed to analyze the stability of the suspensions. The average of the results obtained for the *Pc*AgNPs without and with photoreduction is presented in Table 2. The results indicate that the pH adjustment improves the stability of solutions. *Pc*AgNP6 were the more stable particles. The *Pc*AgNPs kept their stability and colors for at least a year.

3.2 FTIR analysis

Figure 3 and Table 3 present the FTIR spectra obtained for leaf extract and *Pc*AgNPs prepared with leaf and fruit extracts. These spectra can be compared to the spectra obtained by Sampaio et al. [50] for fruit extracts. They observed bands in the region 1600 and 1700 cm^{-1}, an intense stretching peak at 1721 cm^{-1}, and a peak at 1225 cm^{-1}. For spectra measured for *Pc*AgNPs prepared with fruit extract, the same bands are observed (Fig. 3a). In *Pc*AgNPs prepared with leaf extract, it is possible to observe bands at about

Table 2 Zeta potential, particle size, and PDI obtained for *Pc*AgNPs

Sample	Method	Zeta Potential (mV)	Particle size (± SD) (nm)	(PDI)
PcAgNP1	Leaves extract	− 10.8	66.84 ± 45.1	0.455
PcAgNP2	Leaves extract, pH 7.0	− 20.0	44.74 ± 20.54	0.211
PcAgNP3	Leaves extract, Xe	− 17.1	63.70 ± 42.48	0.445
PcAgNP4	Leaves extract, photoreduction, pH 7.0	− 15.5	65.25 ± 31.22	0.252
PcAgNP5	Fruits extract	− 17.1	84.79 ± 45.61	0.289
PcAgNP6	Fruits extract, pH 7.0	− 30.4	104.94 ± 90.20	0.323[a]
PcAgNP7	Fruits extract, Xe	− 20.5	97.72 ± 31.38	0.210[a]
PcAgNP8	Fruits extract, photoreduction, pH 7.0	− 26.7	71.53 ± 36.56	0.261

[a]Measured 5 months after synthesis

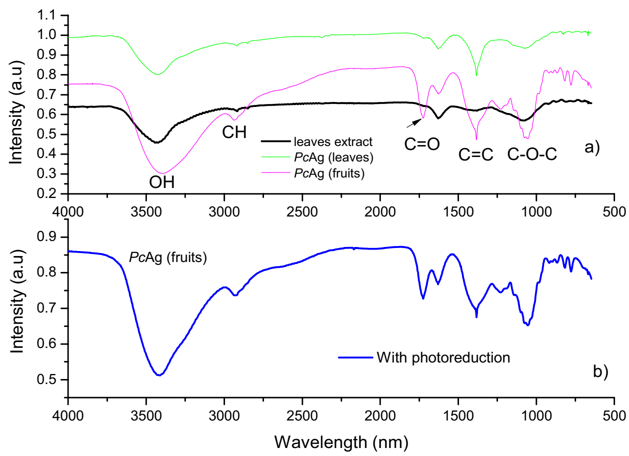

Fig. 3 **a** FTIR spectrum obtained from the *P. cauliflora* leaf extract and *Pc*AgNPs prepared with fruit and leaf extracts with pH 7.0. **b** *Pc*AgNPs prepared with fruit extract with photoreduction and pH 7.0

2919 and 2842 cm^{-1}, indicating the presence of C–H_2 asymmetric and symmetric stretching probably of tannic acid [51]. Also, the band at 1627 cm^{-1} due to the C=C stretching vibrations[52]. The peak observed around 1386 cm^{-1} in fruit extract indicates that the C–H vibration of the different extract compounds interacts significantly with AgNPs. The spectra presented in Fig. 3b of nanoparticles prepared with fruit extract and photoreduction indicated the presence of the same functional groups responsible for the bioreduction of Ag^+ and capping/stabilization.

3.3 Fluorescence analysis

The fluorescence analysis of samples is shown in Fig. 4. Figure 4a shows the emission band of fruit extract due to flavonoids around 440 nm when excited at 320 nm. This figure also shows the fluorescence spectra of *Pc*AgNPs prepared with leaf extract and pH 7.0, showing a shift in emission peak (from ~ 470 nm) and a reduction in intensity compared to the fruit extract emission. Figure 4b shows the excitation and emission spectra (excitations at 300, 320, and 340 nm) obtained for *Pc*AgNPs (fruits extract), presenting a similar spectra profile that one obtained for leaf extract.

3.4 Detection of H_2O_2

A series of H_2O_2 solutions with different concentrations were added to the *Pc*AgNP6 (fruits extract) solution and incubated for 30 min. *Pc*AgNP6 nanoparticles were chosen

Table 3 FTIR peaks obtained from *P. cauliflora* extracts and *Pc*AgNPs

	Plants extracts Wavenumber (cm^{-1})	PcAgNPs Wavenumber (cm^{-1})
O–H stretching	3420	3394
Symmetric and asymmetric vibrational mode of C–H_2 stretching	2919, 2849	2919, 2849
C–H bending		2930
C=O stretching	1721[50]	1727
C=C stretching	1627[52]	1627
C–H bending	1381	1386
C–O stretching	1225[50]	1225
C–O stretching	1082	1057
C–H bending		805

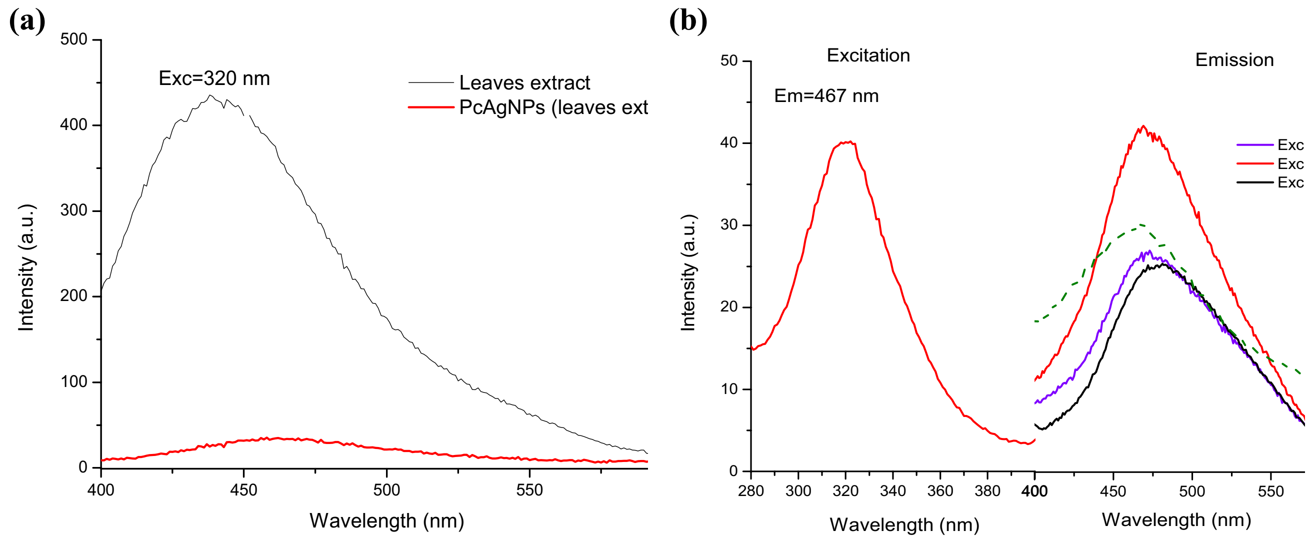

Fig. 4 **a** Fluorescence spectra of leaves and fruit extracts of *P. cauliflora* and *Pc*AgNPs (leaf extract) obtained with excitation at 320 nm. **b** Excitation and emission spectra for *Pc*AgNP (fruit extract)

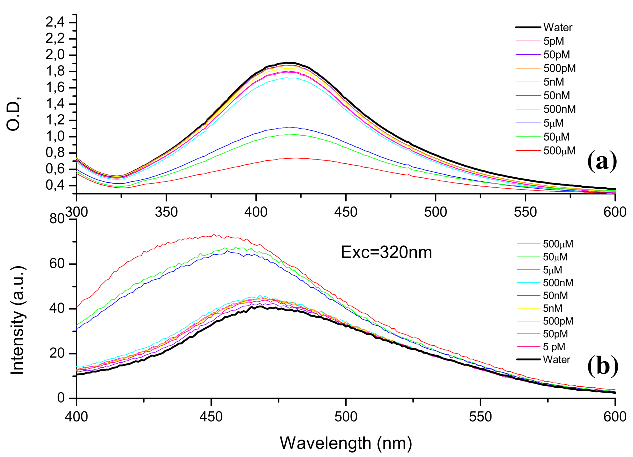

Fig. 5 **a** SPR absorption spectra obtained for *Pc*AgNPs (fruits extract) after reaction with H_2O_2 in various concentrations. **b** Fluorescence spectra obtained with 320 nm excitation after reaction with H_2O_2 in various concentrations for 30 min

for the H_2O_2 detection studies because they have excellent optical properties, stability, and an easy synthesis process. Figure 5a shows the UV–Vis spectra of *Pc*AgNP6 in the presence of H_2O_2, indicating that the SPR peak decreases gradually with the increase in the concentration of H_2O_2. However, Fig. 5b shows an opposite profile in fluorescence spectra, showing an increase in the *Pc*AgNP6 emission band at ~ 460 nm (excitation at 320 nm) with the increase in the concentration of H_2O_2. This result indicates that the luminescence intensity was gradually restored with an increase in the concentration of H_2O_2. Furthermore, a shift in emission peak position could be observed.

The potential use of *Pc*AgNPs as a luminescence sensor for H_2O_2 was studied. A calibration curve obtained from the emission spectra of *Pc*AgNP6 in the presence of H_2O_2 is presented in Fig. 6a. A good linear relationship over the range from 0 to 5 µM with a correlation coefficient of 0.98 was obtained. The limit of detection (LOD) was calculated to be 0.15 µM according to the signal-to-noise method 3σ rule. The detection limit was comparable to H_2O_2 sensors reported in Table 4.

Figure 6b shows the changes in *Pc*AgNPs colloidal solution color in the presence of H_2O_2 with concentrations ranging from ~ 0 to 5 µM, indicating a potential naked-eye colorimetric sensor.

The selectivity of *Pc*AgNPs for H_2O_2 detection was studied. As shown in Fig. 6c, reduced luminescence changes could be observed with the ionic species Ba^{2+}, Ca^{2+}, Cd^{2+}, Co^{2+}, Cu^{+}, K^{+}, Li^{+}, Mg^{2+}, Na^{+}, Sr^{2+}, and Zn^{2+}, compared to results obtained with H_2O_2 with a concentration of 5 µM. In Fig. 6d is observed the *Pc*AgNP6 fluorescence spectra profile in the presence of glucose, cholesterol, triglycerides (present in the blood), urea hydrogen peroxide (present in the urine), tryptophan and saliva. No significant change in *Pc*AgNP fluorescence intensity was observed in the presence of these substances, compared to the changes in the emission intensity and peak wavelength promoted by H_2O_2. These results demonstrate that the *Pc*AgNPs system is selective for H_2O_2 over other non-target substances.

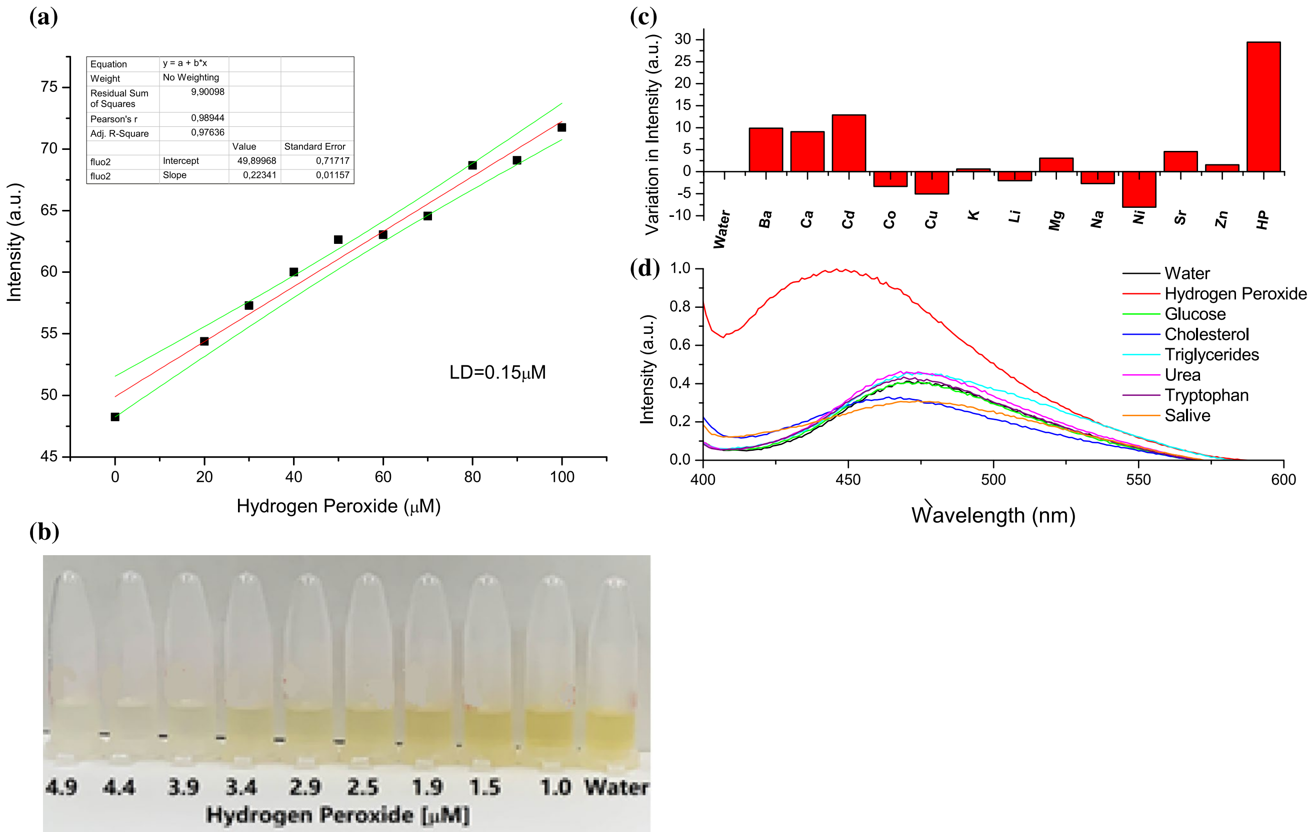

Fig. 6 **a** Fluorescence turn-on calibration curve. **b** The color change of *Pc*AgNPs in the presence of H_2O_2 with concentrations ranging from ~ 5–0 µM. **c** The selectivity of the colorimetric sensing method toward H_2O_2. Variations in luminescence intensity of the *Pc*AgNP system in the presence of interfering species (Ba^{2+}, Ca^{2+}, Cd^{2+}, Co^{2+}, Cu^{+}, K^{+}, Li^{+}, Mg^{2+}, Na^{+}, Sr^{2+}, Zn^{2+}) or H_2O_2. **d** Changes in the fluorescence spectra (excitation at 320 nm) due to glucose, cholesterol, triglycerides, urea hydrogen peroxide, tryptophan, and saliva in *Pc*AgNP6 solution

Table 4 Comparison of analytical performances of different H_2O_2 sensors based on silver nanoparticles

Method limit of detection	Method limit of detection, µM	Linear range, µM	References
Amperometric response	0.24	10–260	[53]
Amperometric response	0.56	0.005–47	[54]
Colorimetric sensor	5.00	75–500	[55]
Colorimetric sensor	3.70	0.45–121	[56]
Fluorescence sensor	0.30	0–17.0	[57]
Colorimetric sensor	0.21	0–140	[58]
Fluorescence turn-on sensor	0.15	0–5.0	This work

4 Discussion

The leaves of *P. cauliflora* possess tannin and flavonoids, quercetin, and myricetin [43, 46]. *P. cauliflora* fruit, jabuticaba, contains carbohydrates, vitamins, minerals, tannins, carotenoids, phenolic acids as ellagic acid, and flavonoids, like quercetin and its isomers, myricetin and anthocyanins, and organic acids as citric acid, succinic acid, malic acid, oxalic acid, and acetic acid [45, 46, 59].

The synthesis of silver nanoparticles from leaf and fruit extracts occurs by reducing the metallic ions to neutral atoms by a redox process promoted by the bioactive compounds present in the extracts [60]. After mixing plant extracts and silver nitrate, the SPR bands are wide, indicating agglomerates. The optical properties of *Pc*AgNPs can be controlled by adjusting the pH to neutral and submitting the solution to the photoreduction process with Xenon illumination. Electrostatic stabilization is regulated by pH adjustment, and the SPR bands become narrowed, indicating monodispersed nanoparticles. Particles can be redispersed by the photoreduction method. Photoreduction offers steric repulsion within nanoparticles, thus preventing the agglomeration and giving rise to a mutual stabilization system. The photoreduction process and pH control increase the Zeta potential value (Table 1), making it more negative, indicating more stable nanoparticles.

The UV–Vis spectra obtained for leaves and fruit extracts presented in Fig. 1a showed that fruit extract has an increased concentration of ellagic acids (EA) and anthocyanins, whereas leaf extract flavonoids such as quercetin [61, 62], and tannic acid[48]. The action of polyphenolic compounds is probably responsible for reducing silver ions and the coating the nanoparticles avoiding their agglomeration [63–65].

Tannic acid mediates the reduction of metal salts and the synthesis of AgNPs. In this case, carboxylic acid groups (COOH) lose their hydrogen atom to become carboxylate ions (COO^-) during the reduction process. The COO^- formed attaches to the surface of silver nanoparticles to act as a surfactant and stabilize AgNPs[66].

Quercetin gives two electrons to Ag^+, forming two AgNPs, with the consequent oxidation of the catechol present on the B ring of the o-quinone group[67].

Ellagic acid reduces silver ions resulting in the formation of AgNPs due to the two-electron oxidation of the hydroxyl groups of the phenol ring system, leading to the formation of a quinoid-containing ketone system [68].

The one-step oxidation–reduction mechanism between Ag^+ and phenolic –OH of anthocyanin leads to Ag^0 [69].

Vibrational bands at 3394 (O–H), 2919 and 2849 ($C–H_2$), 2930 (C–H), 1727 (C=O), 1627 (C=C), 1386 (C–H), 1225 and 1057 (C–O), and 805 and 771 cm^{-1} (C–H), observed in *Pc*AgNPs (Fig. 3), indicate the presence of organic molecules from *P. cauliflora* extracts linked to Ag nanoparticles.

The fluorescence behavior of the studied samples is shown in Fig. 4. Broadband from 380 to 500 nm for leaf extract is due to plant fluorophores[70, 71]. *Pc*AgNPs present a reduction in emission intensity and a shift in the emission peak compared with extracts.

*Pc*AgNPs absorption band in the presence of H_2O_2 gradually decreased with the increase of H_2O_2 concentration, as observed in Fig. 5a. However, the luminescence intensity of the system was gradually restored with an increasing concentration of H_2O_2 (Fig. 5b). The nanoparticles' SPR suppression and luminescence recovery occur immediately after contact with H_2O_2 and stabilize between 10 and 30 min. Therefore, an incubation time of 30 min is recommended before signal reading.

A good linear relationship over the range from 0 to 5 μM was observed in the fluorescence analysis. The critical feature can be observed in the emission peak shift with increased H_2O_2 concentration, making this method sensitive and selective. The sensitivity of this method is compared, as observed in Table 4, to other reported methods for H_2O_2 detection[9, 72].

A schematic representation of H_2O_2 sensing is shown in Fig. 7. The detection mechanism involves a redox reaction between the H_2O_2 and the zero-valent silver. This redox reaction removes the stabilizing agent from the surface of the nanoparticles, facilitating the interaction $H_2O_2–Ag^0$, releasing Ag^+. With this process, the absorbance intensity of the colloidal solution decreases, making the solution colorless. Same time, the luminescence of plant extract polyphenols, which diminishes in the presence of the nanoparticles, is recovered with their destruction. Generally, fluorescence turn-on sensors are less susceptible to false-positive signals than fluorescence quenching sensors [73, 74]. Therefore, *Pc*AgNPs allow both fluorescence turn-on and colorimetric H_2O_2 sensors can be reached.

A dual fluorescence-colorimetric assay for determining the hydrogen peroxide using *Pc*AgNPs was developed. The natural fluorescence of *Plinia caulifora* was quenched upon reaction with AgNPs. Adding hydrogen peroxide to *Pc*AgNPs, the analyte replaced the surface-bound *P. caulifora* molecules, the aggregation of the nanoparticles occurred, corresponding fluorescence reappeared, and a colorimetric variation was observed. The method can be applied to measure the activity of enzymes that generate or eliminate H_2O_2. This allows the screening of compounds that affect the activity of such enzymes as glucose oxidase.

The required instrumentation for the hydrogen peroxide sensor proposed in this work could be a filter-based fluorometer that is simpler, cheaper, and smaller compared to a conventional spectrometer due to the absence of conventional monochromators used for excitation and emission wavelength selection. In this case, an excitation source a light-emitting diode (LED) at 320 nm, an emission filter at ~ 460 nm, and a photosensor are required.

5 Conclusions

This paper presented a simple, fast, non-toxic, eco-friendly, and low-cost process to obtain nanoparticles from *P. cauliflora* leaf and fruit extracts. The formation of the *Pc*AgNPs started immediately after adding $AgNO_3$ to the extracts. The photoreduction process and pH adjustment improve particle qualities. *Pc*AgNPs of the average size of ~ 14 nm are very stable in neutral pH and did not show a significant variation

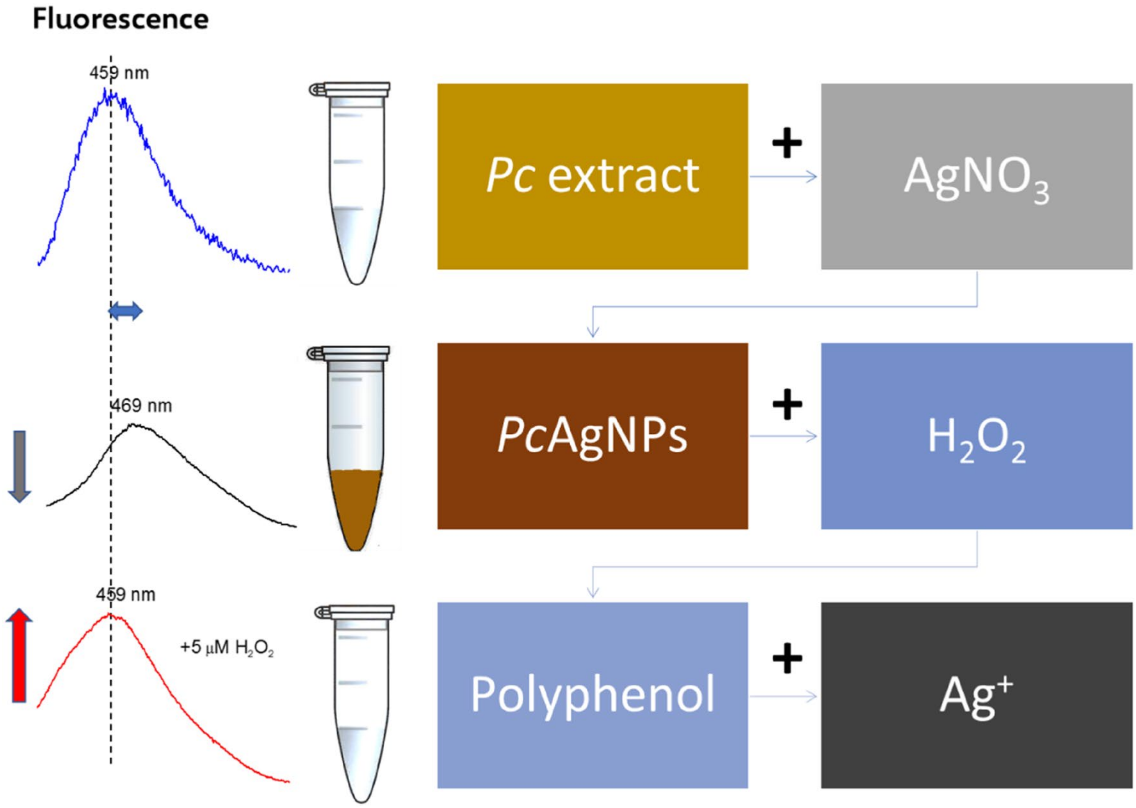

Fig. 7 Schematic representation of H_2O_2 sensing. The synthesis route consists of adding the metallic precursor $AgNO_3$ to the plant extract obtained from the infusion of *Plinia caulifora* fruits in water, followed by pH adjustment. The *Pc* extract solution presents a fluorescence peak around 459 nm due to polyphenols. In *Pc*AgNPs, such fluorescence intensity decreases, and a shift to 469 nm is observed. In the presence of H_2O_2, the SPR band decreases, and the solution returns to its original color depending on H_2O_2 concentration. Nevertheless, polyphenols fluorescence is restored

during 1 year. Comparisons between nanoparticles prepared with leaf and fruit extracts indicated that *Pc*AgNPs prepared with fruits and pH adjustment were the more stable. The fluorescence analysis of *Pc*AgNPs with excitation at 320 nm revealed broadband with a peak around 470 nm due to flavonoids present on the surface of the nanoparticles. With the increased concentration of H_2O_2, the *Pc*AgNPs SPR band gradually decreased, while the luminescence intensity of the system increased. The increase in luminescence occurs from the decomposition of AgNPs by H_2O_2, which restores the emission of plant extract. A shift in the emission peak was also observed in the presence of H_2O_2. To our knowledge, this is the first report of plant-mediated synthesized nanoparticles applied to detect H_2O_2 by fluorescence turn-on method reported in the literature. These finds can be crucial in applying plant-mediated synthesized silver nanoparticles to develop effective fluorescent sensing platforms for label-free sensors.

Funding This work was supported by Grant 303715/2017-0, Conselho Nacional de Desenvolvimento Científico e Tecnológico (CNPq).

Declarations

Conflict of interest The author(s) declared no potential conflicts of interest concerning the research, authorship, and/or publication of this Article.

Credit authorship contribution statement LCC: formal analysis, investigation, validation, resources, writing—original draft. KOG and FROS: data colection.

References

1. J.P. Ribeiro, L.M. Magalhães, M.A. Segundo, S. Reis, J.L. Lima, Hydrogen peroxide, antioxidant compounds and biological targets: an in vitro approach for determination of scavenging capacity using fluorimetric multisyringe flow injection analysis. Talanta **81**(4–5), 1840–1846 (2010). https://doi.org/10.1016/j.talanta.2010.03.049
2. C.L. Hsu, K.S. Chang, J.C. Kuo, Determination of hydrogen peroxide residues in aseptically packaged beverages using an amperometric sensor based on a palladium electrode. Food Control **19**(3), 223–230 (2008). https://doi.org/10.1016/j.foodcont.2007.01.004
3. R. Gradini, C. Fei, T. Richmund, L. Newlin, A summary on cutting edge advancements in sterilization and cleaning technologies in

medical, food, and drug industries, and its applicability to spacecraft hardware. Life Sci. Space Res. **23**, 31–49 (2019). https://doi.org/10.1016/j.lssr.2019.05.002

4. N. Christie-Holmes, R. Tyli, P. Budylowski, F. Guvenc, A. Weiner, B. Poon et al., Vapourized hydrogen peroxide decontamination in a hospital setting inactivates SARS-CoV-2 and HCoV-229E without compromising filtration efficiency of unexpired N95 respirators. Am. J. Infect. Control **49**(10), 1227–1231 (2021). https://doi.org/10.1016/j.ajic.2021.07.012
5. P.V. Mohanan, V. Sangeetha, A. Sabareeswaran, V. Muraleedharan, K. Jithin, U. Vandana et al., Safety of 0.5% hydrogen peroxide mist used in the disinfection gateway for COVID-19. Environ. Sci. Pollut. Res. **28**(47), 66602–66612 (2022). https://doi.org/10.1007/s11356-021-15164-y
6. C.Y.S. Chung, G.A. Timblin, K. Saijo, C.J. Chang, Versatile histochemical approach to detection of hydrogen peroxide in cells and tissues based on puromycin staining. J. Am. Chem. Soc. **140**(19), 6109–6121 (2018). https://doi.org/10.1021/jacs.8b02279
7. A. Abdalla, W. Jones, M.S. Flint, B.A. Patel, Bicomponent composite electrochemical sensors for sustained monitoring of hydrogen peroxide in breast cancer cells. Electrochim. Acta (2021). https://doi.org/10.1016/j.electacta.2021.139314
8. 46th ESAO Congress 3-7 September 2019 Hannover, Germany Abstracts. Int. J. Artif. Organs. 2019;42(8):386–474. https://doi.org/10.1177/0391398819860985
9. J. Meier, E.M. Hofferber, J.A. Stapleton, N.M. Iverson, Hydrogen peroxide sensors for biomedical applications. Chemosensors. (2019). https://doi.org/10.3390/chemosensors7040064
10. C.P. Ge, Y. Yan, P.F. Tan, S. Hu, Y.B. Jin, Y.Y. Shang et al., A NIR fluorescent probe for the in vitro and in vivo selective detection of hydrogen peroxide. Sens. Actuators B Chem. (2022). https://doi.org/10.1016/j.snb.2021.130831
11. E. Tan, İ Kahyaoğlu, S. Karakuş, A sensitive and smartphone colorimetric assay for the detection of hydrogen peroxide based on antibacterial and antifungal matcha extract silver nanoparticles enriched with polyphenol. Polym. Bull. (Berl.) (2021). https://doi.org/10.1007/s00289-021-03857-w
12. Z.S. Jie, J. Liu, M.C. Shu, Y. Ying, H.F. Yang, Detection strategies for superoxide anion: a review. Talanta (2022). https://doi.org/10.1016/j.talanta.2021.122892
13. H. Chu, L. Yang, L. Yu, J. Kim, J. Zhou, M. Li et al., Fluorescent probes in public health and public safety. Coord. Chem. Rev. (2021). https://doi.org/10.1016/j.ccr.2021.214208
14. V.N. Nguyen, J. Ha, M. Cho, H.D. Li, K.M.K. Swamy, J. Yoon, Recent developments of BODIPY-based colorimetric and fluorescent probes for the detection of reactive oxygen/nitrogen species and cancer diagnosis. Coord. Chem. Rev. (2021). https://doi.org/10.1016/j.ccr.2021.213936
15. C.R.B. Lopes, D. Santos, F.R.D. Silva, L.C. Courrol, High-sensitivity Hg^{2+} sensor based on the optical properties of silver nanoparticles synthesized with aqueous leaf extract of *Mimusops coriacea*. Appl. Phys. A Mater. Sci. Process. (2021). https://doi.org/10.1007/s00339-021-04391-2
16. D. Sun, D. Yang, P. Wei, B. Liu, Z. Chen, L. Zhang et al., One-step electrodeposition of silver nanostructures on 2D/3D metal-organic framework ZIF-67: comparison and application in electrochemical detection of hydrogen peroxide. ACS Appl Mater Interfaces **12**(37), 41960–41968 (2020). https://doi.org/10.1021/acsami.0c11269
17. S. Teerasong, T. Sonsa-Ard, C. Vimolkanjana, N. Choengchan, A. Chompoosor, D. Nacapricha, Colorimetric sensor using silver nanoparticles for determination of hydrogen peroxide based on a flow injection system. J. Nanoelectron. Optoelectron. **8**(5), 446–449 (2013). https://doi.org/10.1166/jno.2013.1506
18. A. Kalai Priya, G.K. Yogesh, K. Subha, V. Kalyanavalli, D. Sastikumar, Synthesis of silver nano-butterfly park by using laser ablation of aqueous salt for gas sensing application. Appl. Phys. A Mater. Sci. Process. (2021). https://doi.org/10.1007/s00339-021-04370-7
19. V.V. Apyari, E.A. Terenteva, A.R. Kolomnikova, A.V. Garshev, S.G. Dmitrienko, Y.A. Zolotov, Potentialities of differently-stabilized silver nanoparticles for spectrophotometric determination of peroxides. Talanta **202**, 51–58 (2019). https://doi.org/10.1016/j.talanta.2019.04.056
20. M. Bilal, T. Rasheed, H.M.N. Iqbal, H.B. Hu, X.H. Zhang, Silver nanoparticles: biosynthesis and antimicrobial potentialities. Int. J. Pharmacol. **13**(7), 832–845 (2017). https://doi.org/10.3923/ijp.2017.832.845
21. N.M. Alabdallah, M.M. Hasan, Plant-based green synthesis of silver nanoparticles and its effective role in abiotic stress tolerance in crop plants. Saudi J. Biol. Sci. **28**(10), 5631–5639 (2021). https://doi.org/10.1016/j.sjbs.2021.05.081
22. M. Ghaffari-Moghaddam, R. Hadi-Dabanlou, M. Khajeh, M. Rakhshanipour, K. Shameli, Green synthesis of silver nanoparticles using plant extracts. Korean J. Chem. Eng. **31**(4), 548–557 (2014). https://doi.org/10.1007/s11814-014-0014-6
23. N. Kannan, S. Subbalaxmi, Biogenesis of nanoparticles—a current perspective. Rev. Adv. Mater. Sci. **27**(2), 99–114 (2011)
24. Priya AK, Rao SK, Yogesh GK, Rohini P, Sastikumar D. Green synthesis of Silver Nanoparticles by Pulsed Laser ablation using Citrus Limetta juice extract for Clad-Modified Fiber Optic gas sensing application. Conference on Nanoengineering - Fabrication, Properties, Optics, Thin Films, and Devices XVIII. San Diego, CA (2021)
25. Priya AK, Sastikumar D. Nano-second Pulsed Laser Ablation and Transformation of Bulk Titanium dioxide (TiO2) into Nano-Particles for Fiber Optic Gas Sensor. 64th DAE Solid State Physics Symposium (DAE-SSPS). Indian inst Technol Jodhpur, Jodhpur, INDIA2019.
26. C.R. Borges, R.E. Samad, K.D. Goncalves, D.P. Vieira, L.C. Courrol, Interaction between protoporphyrin IX and tryptophan silver nanoparticles. J. Nanopart. Res. (2018). https://doi.org/10.1007/s11051-018-4269-4
27. Kshirsagar P, Sangaru SS, Malvindi MA, Martiradonna L, Cingolani R, Pompa PP. Synthesis of highly stable silver nanoparticles by photoreduction and their size fractionation by phase transfer method. Colloids and Surfaces A Physicochemical and Engineering Aspects. 2011;392(1):264–70. doi: https://doi.org/10.1016/j.colsurfa.2011.10.003.
28. C.R.B. Lopes, L.C. Courrol, Green synthesis of silver nanoparticles with extract of *Mimusops coriacea* and light. J. Lumin. **199**, 183–187 (2018). https://doi.org/10.1016/j.jlumin.2018.03.030
29. D.D. Courrol, C.R.B. Lopes, T.D. Cordeiro, M.R. Franzolin, N.D. Vieira, R.E. Sarnad et al., Optical properties and antimicrobial effects of silver nanoparticles synthesized by femtosecond laser photoreduction. Opt. Laser Technol. **103**, 233–238 (2018). https://doi.org/10.1016/j.optlastec.2018.01.044
30. R.A. de Matos, L.C. Courrol, Biocompatible silver nanoparticles prepared with amino acids and a green method. Amino Acids **49**(2), 379–388 (2017). https://doi.org/10.1007/s00726-016-2371-4
31. K.D. Goncalves, F.R.D. Silva, D.P. Vieira, L.C. Courrol, Synthesis and characterization of aminolevulinic acid with gold and iron nanoparticles by photoreduction method for non-communicable diseases diagnosis and therapy. J. Mater. Sci. Mater. Electron. **30**(18), 16789–16797 (2019). https://doi.org/10.1007/s10854-019-01337-6
32. J.L. Gardea-Torresdey, E. Gomez, J.R. Peralta-Videa, J.G. Parsons, H. Troiani, M. Jose-Yacaman, Alfalfa sprouts: a natural source for the synthesis of silver nanoparticles. Langmuir **19**(4), 1357–1361 (2003). https://doi.org/10.1021/la020835i

33. M. Yilmaz, H. Turkdemir, M.A. Kilic, E. Bayram, A. Cicek, A. Mete et al., Biosynthesis of silver nanoparticles using leaves of *Stevia rebaudiana*. Mater. Chem. Phys. **130**(3), 1195–1202 (2011). https://doi.org/10.1016/j.matchemphys.2011.08.068
34. V. Gopinath, D. MubarakAli, S. Priyadarshini, N.M. Priyadharsshini, N. Thajuddin, P. Velusamy, Biosynthesis of silver nanoparticles from Tribulus terrestris and its antimicrobial activity: a novel biological approach. Colloids Surf. B Biointerfaces **96**, 69–74 (2012). https://doi.org/10.1016/j.colsurfb.2012.03.023
35. M. Vanaja, G. Annadurai, *Coleus aromaticus* leaf extract mediated synthesis of silver nanoparticles and its bactericidal activity. Appl. Nanosci. **3**(3), 217–223 (2013). https://doi.org/10.1007/s13204-012-0121-9
36. P.M. Mishra, L. Sundaray, G.K. Naik, K.M. Parida, Biomimetic synthesis of silver nanoparticles by aqueous extract of *Cinnamomum tamala* leaves: optimization of process variables. Nanosci. Nanotechnol. Lett. **6**(5), 409–414 (2014). https://doi.org/10.1166/nnl.2014.1771
37. S.M. Amini, Preparation of antimicrobial metallic nanoparticles with bioactive compounds. Mater. Sci. Eng. C Mater. Biol. Appl. (2019). https://doi.org/10.1016/j.msec.2019.109809
38. G. Oza, A. Reyes-Calderon, A. Mewada, L.G. Arriaga, G.B. Cabrera, D.E. Luna, et al., Plant-based metal and metal alloy nanoparticle synthesis: a comprehensive mechanistic approach. J. Mater. Sci. https://doi.org/10.1007/s10853-019-04121-3
39. M.R. Franzolin, DdSC, SdSB, A.L.C. Courrol, *Eugenia uniflora* L. silver and gold nanoparticle synthesis, characterization, and evaluation of the photoreduction process in antimicrobial activities. Microorganisms (2022). https://doi.org/10.3390/microorganisms10050999
40. D.T. Santos, P.C. Veggi, M.A.A. Meireles, Extraction of antioxidant compounds from Jabuticaba (*Myrciaria cauliflora*) skins: yield, composition and economical evaluation. J. Food Eng. **101**(1), 23–31 (2010). https://doi.org/10.1016/j.jfoodeng.2010.06.005
41. A.D.J. Boari Lima, A.D. Correa, A.P. Carvalho Alves, C.M. Patto Abreu, A.M. Dantas-Barros, Chemical characterization of the jabuticaba fruits (*Myrciaria cauliflora* Berg) and their fractions. Arch. Latinoam. Nutr. **58**(4), 416–421 (2008)
42. J.C. Baldin, E.C. Michelin, Y.J. Polizer, I. Rodrigues, S.H. Seraphin de Godoy, R.P. Fregonesi et al., Microencapsulated jabuticaba (*Myrciaria cauliflora*) extract added to fresh sausage as natural dye with antioxidant and antimicrobial activity. Meat Sci. **118**, 15–21 (2016). https://doi.org/10.1016/j.meatsci.2016.03.016
43. T.M. Souza-Moreira, J.A. Severi, E.R. Rodrigues, M.I. de Paula, J.A. Freitas, W. Vilegas et al., Flavonoids from *Plinia cauliflora* (Mart.) Kausel (Myrtaceae) with antifungal activity. Nat. Prod. Res. **33**(17), 2579–2582 (2019). https://doi.org/10.1080/14786419.2018.1460827
44. G. Mannino, A. Perrone, C. Campobenedetto, A. Schittone, C.M. Bertea, C. Gentile, Phytochemical profile and antioxidative properties of *Plinia trunciflora* fruits: a new source of nutraceuticals. Food Chem. **307**, 8 (2020). https://doi.org/10.1016/j.foodchem.2019.125515
45. A.G. Junior, P. de Souza, F.A.D. Livero, *Plinia cauliflora* (Mart) Kausel: a comprehensive ethnopharmacological review of a genuinely Brazilian species. J. Ethnopharmacol. (2019). https://doi.org/10.1016/j.jep.2019.112169
46. A.D.J. Boari Lima, A.D. Correa, A.A. Saczk, M.P. Martins, R.O. Castilho, Anthocyanins, pigment stability and antioxidant activity in jabuticaba *Myrciaria cauliflora* (Mart.) O. Berg. Rev. Bras. Frutic. **33**(3), 877–887 (2011)
47. K. Csepregi, M. Kocsis, E. Hideg, On the spectrophotometric determination of total phenolic and flavonoid contents. Acta Biol. Hung. **64**(4), 500–509 (2013). https://doi.org/10.1556/ABiol.64.2013.4.10
48. Z. Jurasekova, J.V. Garcia-Ramos, C. Domingo, S. Sanchez-Cortes, Surface-enhanced Raman scattering of flavonoids. J. Raman Spectrosc. **37**(11), 1239–1241 (2006). https://doi.org/10.1002/jrs.1634
49. M. Hasegawa, M. Terauchil, Y. Kikuchi, A. Nakao, J. Okubo, T. Yoshinaga et al., Deprotonation processes of ellagic acid in solution and solid states. Monatshefte Fur Chemie **134**(6), 811–821 (2003). https://doi.org/10.1007/s00706-002-0552-1
50. D.M. Sampaio, R.S. Babu, H.R.M. Costa, A.L.F. de Barros, Investigation of nanostructured TiO_2 thin film coatings for DSSCs application using natural dye extracted from jabuticaba fruit as photosensitizers. Ionics **25**(6), 2893–2902 (2019). https://doi.org/10.1007/s11581-018-2753-6
51. T.K. Patle, K. Shrivas, R. Kurrey, S. Upadhyay, R. Jangde, R. Chauhan, Phytochemical screening and determination of phenolics and flavonoids in Dillenia pentagyna using UV-Vis and FTIR spectroscopy. Spectrochimica Acta Part A Mol. Biomol. Spectrosc. (2020). https://doi.org/10.1016/j.saa.2020.118717
52. I.O. Faniyi, O. Fasakin, B. Olofinjana, A.S. Adekunle, T.V. Oluwasusi, M.A. Eleruja et al., The comparative analyses of reduced graphene oxide (RGO) prepared via green, mild and chemical approaches. Sn Appl. Sci. (2019). https://doi.org/10.1007/s42452-019-1188-7
53. A.A. Abdelwahab, Y.B. Shim, Nonenzymatic H_2O_2 sensing based on silver nanoparticles capped polyterthiophene/MWCNT nanocomposite. Sens. Actuators B Chem. **201**, 51–58 (2014). https://doi.org/10.1016/j.snb.2014.05.004
54. Y. Li, P.P. Zhang, Z.F. Ouyang, M.F. Zhang, Z.J. Lin, J.F. Li et al., Nanoscale graphene doped with highly dispersed silver nanoparticles: quick synthesis, facile fabrication of 3d membrane-modified electrode, and super performance for electrochemical sensing. Adv. Funct. Mater. **26**(13), 2122–2134 (2016). https://doi.org/10.1002/adfm.201504533
55. Z.B. Xiang, Y. Wang, P. Ju, D. Zhang, Optical determination of hydrogen peroxide by exploiting the peroxidase-like activity of AgVO3 nanobelts. Microchim. Acta **183**(1), 457–463 (2016). https://doi.org/10.1007/s00604-015-1670-x
56. A. Elgamouz, K. Bajou, B. Hafez, C. Nassab, A. Behi, M. Abu Haija et al., Optical sensing of hydrogen peroxide using starch capped silver nanoparticles, synthesis, optimization and detection in urine. Sens. Actuators Rep. (2020). https://doi.org/10.1016/j.snr.2020.100014
57. J.S. Liu, Z.Z. Dong, C. Yang, G.D. Li, C. Wu, F.W. Lee et al., Turn-on luminescent probe for hydrogen peroxide sensing and imaging in living cells based on an iridium(III) complex-silver nanoparticle platform. Sci Rep. (2017). https://doi.org/10.1038/s41598-017-09478-6
58. A. Ruby, M.S. Mehata, Surface plasmon resonance allied applications of silver nanoflowers synthesized from Breynia vitis-idaea leaf extract. Dalton Trans. **51**(7), 2726–2736 (2022). https://doi.org/10.1039/d1dt03592d
59. D. Helena, M.B. Andressa, F.F.A. Celio, M.P. Glaucia, B.B.C. Cinthia, R.M. Mario, Influence of different types of acids and pH in the recovery of bioactive compounds in Jabuticaba peel (*Plinia cauliflora*). Food Res. Int. **124**, 16–26 (2019). https://doi.org/10.1016/j.foodres.2019.01.010
60. P.W. Connelly, D. Draganov, G.F. Maguire, Paraoxonase-1 does not reduce or modify oxidation of phospholipids by peroxynitrite. Free Radic. Biol. Med. **38**(2), 164–174 (2005). https://doi.org/10.1016/j.freeradbiomed.2004.10.010
61. Y.S. Liu, Y.C. Chang, H.H. Chen, Silver nanoparticle biosynthesis by using phenolic acids in rice husk extract as reducing agents and dispersants. J. Food Drug Anal. **26**(2), 649–656 (2018). https://doi.org/10.1016/j.jfda.2017.07.005

62. N.D. Neves, P.C. Stringheta, I.F. da Silva, E. Garcia-Romero, S. Gomez-Alonso, I. Hermosin-Gutierrez, Identification and quantification of phenolic composition from different species of Jabuticaba (*Plinia* spp.) by HPLC-DAD-ESI/MSn. Food Chem. (2021). https://doi.org/10.1016/j.foodchem.2021.129605
63. E. Bulut, M. Ozacar, Rapid, facile synthesis of silver nanostructure using hydrolyzable tannin. Ind. Eng. Chem. Res. **48**(12), 5686–5690 (2009). https://doi.org/10.1021/ie801779f
64. Y.S. Rao, V.S. Kotakadi, T. Prasad, A.V. Reddy, D. Gopal, Green synthesis and spectral characterization of silver nanoparticles from Lakshmi tulasi (*Ocimum sanctum*) leaf extract. Spectrochimica Acta Part A Mol. Biomol. Spectrosc. **103**, 156–159 (2013). https://doi.org/10.1016/j.saa.2012.11.028
65. S. Rajeshkumar, L.V. Bharath, Mechanism of plant-mediated synthesis of silver nanoparticles—a review on biomolecules involved, characterisation and antibacterial activity. Chem. Biol. Interact. **273**, 219–227 (2017). https://doi.org/10.1016/j.cbi.2017.06.019
66. T.Y. Kim, S.H. Cha, S. Cho, Y. Park, Tannic acid-mediated green synthesis of antibacterial silver nanoparticles. Arch Pharm Res. **39**(4), 465–473 (2016). https://doi.org/10.1007/s12272-016-0718-8
67. F. Tasca, R. Antiochia, Biocide activity of green quercetin-mediated synthesized silver nanoparticles. Nanomaterials (2020). https://doi.org/10.3390/nano10050909
68. S.N. Barnaby, S.M. Yu, K.R. Fath, A. Tsiola, O. Khalpari, I.A. Banerjee, Ellagic acid promoted biomimetic synthesis of shape-controlled silver nanochains. Nanotechnology **22**(22), 225605 (2011). https://doi.org/10.1088/0957-4484/22/22/225605
69. S.A. Al-Thabaiti, Z. Khan, Biogenic synthesis of silver nanoparticles, sensing and photo catalytic activities for bromothymol blue. J. Photochem. Photobiol **3-4**, 100010 (2020). https://doi.org/10.1016/j.jpap.2020.100010
70. S.L. Smith, K.M. Nissamudeen, D. Philip, K.G. Gopchandran, Studies on surface plasmon resonance and photoluminescence of silver nanoparticles. Spectrochimica Acta Part A Mol. Biomol. Spectrosc. **71**(1), 186–190 (2008). https://doi.org/10.1016/j.saa.2007.12.002
71. Z. Parang, A. Keshavarz, S. Farahi, S.M. Elahi, M. Ghoranneviss, S. Parhoodeh, Fluorescence emission spectra of silver and silver/cobalt nanoparticles. Scientia Iranica **19**(3), 943–947 (2012). https://doi.org/10.1016/j.scient.2012.02.026
72. U. Anik, S. Timur, Z. Dursun, Metal organic frameworks in electrochemical and optical sensing platforms: a review. Microchim. Acta (2019). https://doi.org/10.1007/s00604-019-3321-0
73. Y.X. Liao, K. Li, M.Y. Wu, T. Wu, X.Q. Yu, A selenium-contained aggregation-induced "turn-on" fluorescent probe for hydrogen peroxide. Org. Biomol. Chem. **12**(19), 3004–3008 (2014). https://doi.org/10.1039/c4ob00206g
74. J.S. Liu, G.N. Liu, W.X. Liu, Y.R. Wang, Turn-on fluorescence sensor for the detection of heparin based on rhodamine B-modified polyethyleneimine-graphene oxide complex. Biosens. Bioelectron. **64**, 300–305 (2015). https://doi.org/10.1016/j.bios.2014.09.023